Corrosion and Wear Resistance of Chrome White Irons—A Correlation to Their Composition and Microstructure

BAOTONG LU, JINGLI LUO, and STEFANO CHIOVELLI

The corrosion and wear resistances of a series of cast chromium white irons (CWIs) were evaluated using electrochemical and low stress sliding abrasion tests. The results show clearly that corrosion resistance of these materials is largely dependent on the quantity of chromium in the matrix, while wear resistance is mainly controlled by the volume fraction of chromium carbides. Based on theoretical analysis, a wear/corrosion performance map is established to identify alloy compositions that may be suited for erosion/corrosion conditions.

I. INTRODUCTION

EROSION corrosion causes a serious problem for the oil sands industry of Northern Alberta, Canada, where handling and processing of essentially silica-based solids results in extremely severe wear conditions.[1] Proper materials selection with a good wear resistance is an effective way to extend the service life of slurry components and to reduce overall maintenance as well as capital expenditures. Chrome white irons (CWIs) and their overlays are specifically developed for abrasion-resistant applications,[2] because of their excellent abrasive resistance and moderate ability against impact, which is necessary for crushing, grinding, and slurry erosion applications.[3,4,5] These alloys are readily castable. The carbides present in microstructure, mainly in the form of M_7C_3, provide high hardness and wear resistance.[6,7,10] The high chromium content of CWIs is adopted to prevent the formation of graphite and to ensure the stability of the carbides, as well as air hardenability. Copper, manganese, nickel, and molybdenum are typically added to suppress the formation of pearlite on cooling.[8] The matrix structure is adjusted by heat treatment and alloy content to balance wear properties and toughness.

A large body of articles can be found on the wear behavior of cast CWIs[2,5,9–11] and several models have been developed for the microstructure-property relationship of these alloys.[12,13] However, the slurries in the oil sand production are often corrosive. The information on the performance of CWIs in the corrosive environments is yet limited in the open literature,[13,14,15] although experimental evidence has indicated that CWIs with high mechanical strength are less resistant to corrosion[13] and these alloys become less resistant to wear when corrosion is present.[10,15,16] To optimize the material performance under the service conditions, the effects of the chemical composition and microstructure on the property of material should be well understood.

The present work investigates the corrosion and low stress sliding-wear resistance of a family of CWI materials typically used in slurry pump applications to establish relationships between chemical composition, microstructure, wear, and the corrosion resistance of these alloys. An attempt was made to propose a criterion for material selection based on the concept of a wear/corrosion performance map.

BAOTONG LU, Visiting Professor, and JINGLI LUO, Professor, are with Department of Chemical and Materials Engineering, University of Alberta, Edmonton, AB, T6G 2G6 Canada. STEFANO CHIOVELLI, Senior Associate Engineer, is with Syncrude Canada Ltd., Edmonton, AB, T6N 1H4. Contact e-mail: jjingli.luo@ualberta.ca

Manuscript submitted May 3, 2005.

II. EXPERIMENTAL

A. *Test Materials*

Test materials were 12 commercial CWI castings. The basic compositions are listed in Table I and shown in the austenite liquidus surface diagram for the Fe-rich corner of the Fe-Cr-C phase diagram (Figure 1).[8,17] Some microstructural parameters and the microhardness of the matrix Hv_M are also listed in Table I. The matrix structures of materials were identified using the metallographic techniques and microhardness measurements of the matrix. The microhardness of constitutes in the microstructures were measured with a Shimazhu (Japan) microhardness tester (100-mg load). The volume fraction of carbides in the microstructure, pct K, was measured by an Image-Pro Plus system (Media Cybemetic Co., U.S.). These alloys can be further categorized as hypo-eutectic, eutectic, or hyper-eutectic. The typical microstructures of as-tested materials are described in Figure 2.

B. *Polarization Resistance Measurements*

The test solution was the process recycle cooling water, which was used for the oil sand production in Northern Alberta, Canada. It contained Cl^-, SO_4^{2-}, S^{2-}, and other corrosive species, as listed in Table II. Before the corrosion tests, samples were embedded in an epoxy resin. The edges of each sample were coated with an acrylic paint in order to avoid crevice corrosion between the sample and epoxy resin. Prior to each measurement, the test surface was successively ground with silicon carbide (SiC) papers of 240, 400, and 600 grit and then rinsed with deionized water and acetone.

The polarization resistance R_p was used in the current investigation to evaluate the corrosion resistance of material since the corrosion current density can simply relate to the polarization resistance as

$$i_{\text{corr}} = \frac{B}{R_p} \qquad [1]$$

where B is a constant depending on the corrosion system. The polarization resistance measurements were performed

Table I. Basic Compositional and Microstructural Parameters of Testing Materials

SCL ID	Basic Composition (Wt Pct)				Pct Cr_M (Wt Pct)	Pct K (Vol Pct)	Hv_M	Matrix Structure
	C	Cr	Mo	Ni				
EAN	3.2	9.6	0.2	5.06	4.91	29.8	670	P + M
ECP							752	P + M
ECO							741	P + M
EAD	2.9	20.8	1.5	0.92	10.1	33.0	423	A
ECN							572	A
EAS	3.9	38.8	0.3	0.48	14.6	51.8	761	M
ECM							419	A
EAP	2.5	25.8	0.6	0.47	13.4	29.0	725	P + M
EAQ	2.1	25.8	0.04	2.26	14.4	24.6	495	A
EAR	2.0	32.0	2.5	2.47	18.2	23.5	380	A
ECL							508	A
EAT	1.7	38.4	1.8	6.41	22.5	22.0	409	A

Pct Cr_M: chromium contents in matrix.
Pct K: volume fraction of carbides.
Hv_M: microhardness of matrix.
P: pearlite, M: martensite, and A: austenite.

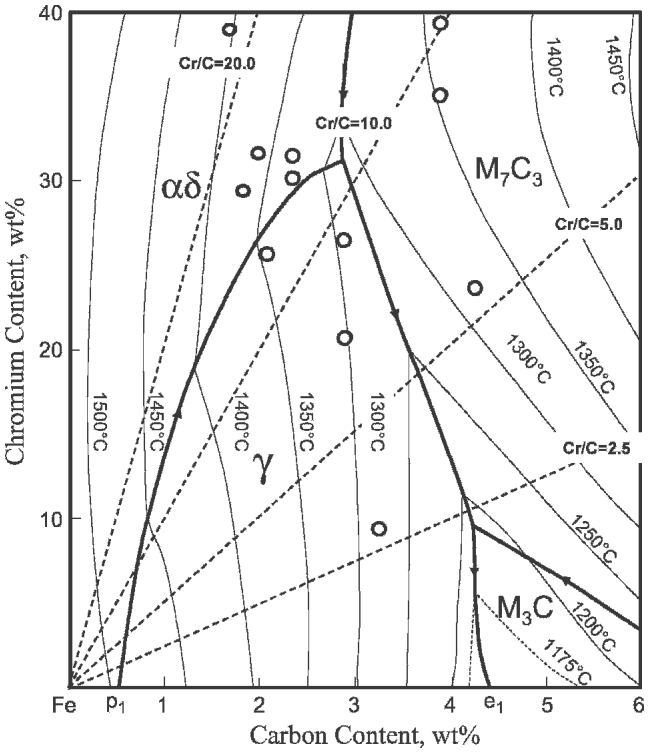

Fig. 1—Alloys studied *vs* austenite liquidus surface diagram for the Fe-rich corner of the Fe-Cr-C ternary system.[9,10]

in a 1000-mL EG&G corrosion cell using a Solartron (U.S.) 1287 potentiostat. A long coiled platinum wire was used as the counterelectrode and a saturated calomel electrode (SCE) was used as the reference electrode. The SCE was led to the surface of the working electrode with a Luggin capillary. The polarization resistance was measured with a potential scanning rate of 0.2 $mV \cdot s^{-1}$ within the potential range of $E_{corr} \pm 10$ mV. The term E_{corr} is the open circuit potential of material under the test condition.

The measurements were performed at room temperature (22 °C) and 60 °C with a fluctuation less than ±1 °C under both aerated and deaerated conditions. The deaerated condition was created by continuously bubbling nitrogen for 3 hours before each measurement, and this condition was held unchanged during the test. Air was bubbled continuously into the test solution to create the aerated condition. Dissolved oxygen concentration (DOC) in tailing solution was measured using a M407510 Dissolved Oxygen Meter (Extec Instruments, U.S.). It was found that the DOC at 22 °C was 10 mg/L in the aerated tailing solution and less than 0.1 mg/L under the deaerated condition. The DOC at 60 °C was not measured because the temperature is out of the operating temperature range of the oxygen probe (≤50 °C).

C. *Wear Tests*

The wear resistance of materials was evaluated with the low stress abrasion dry sand rubber wheel test according to procedure A in ASTM G65. This test simulates low stress sliding abrasion, which is typical on chutes, hoppers, and ground engaging tools and has also been found to be a useful screening test for some slurry erosion applications. Figure 3 shows the experimental setup for the wear test. The sand was commercially available silica sand (U.S. Silica Company, Ottawa) with size of 50 to 70 mesh (300 to 212 μm). The abrasive flow rate was 300 to 400 g/min, the test load was 130 N, and the number the revolutions of the rubber wheel was 6000, which corresponded to the total sliding distance 4309 m. The wear rate of material was given by the volume loss/sliding distance (mm^3/m).

III. RESULTS AND DISCUSSION

A. *Effects of Chemical Composition and Microstructure on Wear Resistance*

The data in Figure 4 show that the wear rate of the test materials depends heavily on their carbon content. In the

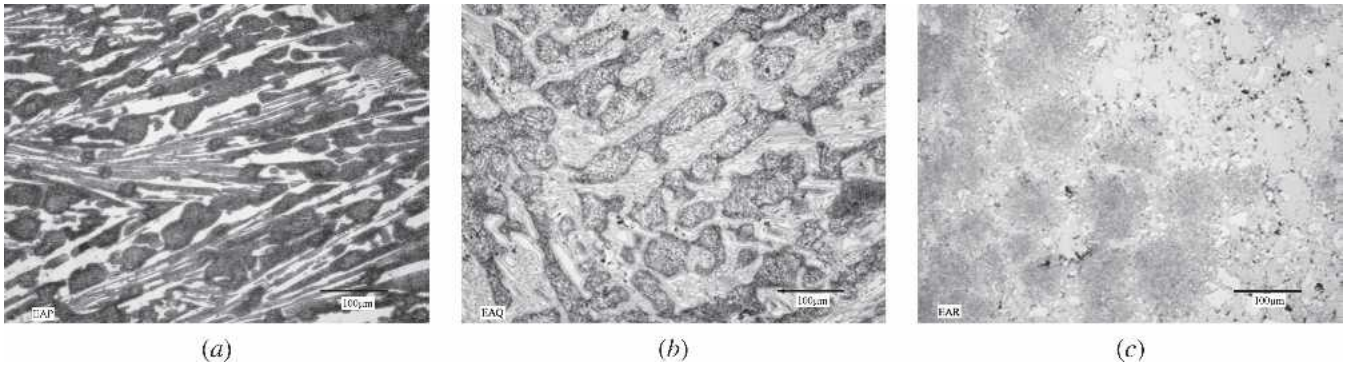

Fig. 2—Typical microstructures of testing materials: (*a*) EAP (hypereutectic CWI), (*b*) EAQ (eutectic CWI), and (*c*) EAQ (hypoeutectic CWI).

Table II. Chemical Composition of the Process Recycle-Cooling Water (pH = 8.05)

Cation	Na^+	K^+	Ca^{2+}	Mg^{2+}
mg/L	727	11.3	6.8	4.0
Anion	Cl^-	SO_4^{2-}	HCO_3^-	CO_3^{2-}
mg/L	380	211	950	<5

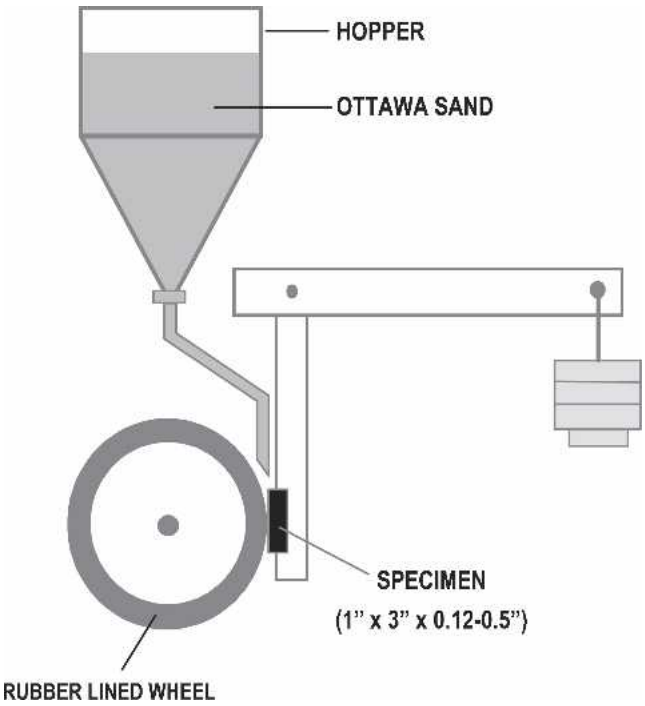

Fig. 3—ASTM G65 dry sand rubber wheel tester.

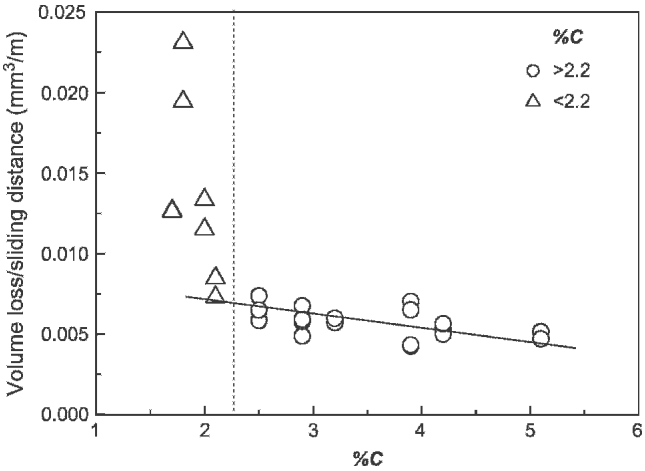

Fig. 4—Effects of carbon content on wear resistance.

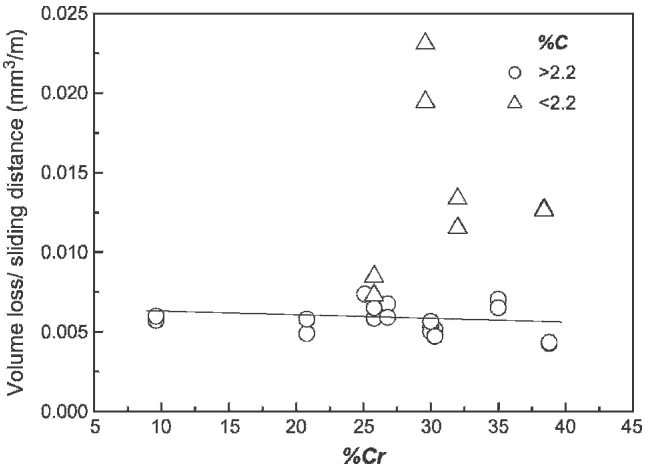

Fig. 5—Effects of chromium content on wear resistance.

range of pct C $\geq$ 2.2, the wear resistance degrades gradually with the carbon content, but when pct C $<$ 2.2, the wear resistance decreases sharply. However, the wear rate of testing materials is essentially independent of chromium content, as indicated in by Figure 5. Three samples with high Cr content in Figure 5 display a high material loss rate due to their low carbon content (pct C $<$ 2.2).

According to the microhardness measurements, the hardness of the carbides in the test materials was in the range of 1000 to 1500 Hv, which falls in the hardness range of M_7C_3/M_3C and is higher than that of silica sand used in our test (840 Hv).[12] Other researchers have concluded that when the hardness of the erodent (50/70 Ottawa silica sand) is lower than that of carbides in the microstructure, the wear resistance of CWI will increase with increasing carbide volume fraction.[12] It has also been well documented that the carbide volume fraction is approximately proportional to the carbon content of materials.[17] The test results in

Figure 6 indicate that there is a wear mechanism transition at a critical carbide content, pct K_C (≈28 pct). When pct K > pct K_C, the material loss rate decreases slowly with increasing volume fraction of carbides, but when the pct K < pct K_C, it increases abruptly with decreasing volume fraction of carbides. Such a phenomenon may relate to the wear mechanism transition owing to the change in the relative size of abrasive and average distance between carbides.[12] When the volume fraction of carbides is above the critical value, the equivalent distance between carbides is quite small compared with the average size of sand particles and the wear process will likely occur in a uniform mode. In this case, the wear rate depends mainly on the relative hardness of carbides and erodent and the role of the relatively soft matrix is to mainly provide mechanical support to carbides. If the volume fraction of carbides is below the critical value, the equivalent distance between carbides become comparable with the erodent size and the matrix region will be worn preferentially, resulting in a high material loss rate owing to the fast removal of the matrix and subsequently unsupported carbides.[12] The three samples (EAR, ECL, and EAT) displaying relatively poor wear resistance belong to the hypoeutectic CWI family. Since these alloys lack primary carbides, the average sizes of carbides in these materials are much smaller and the distance between the carbides is greater than those in the hypereutectic CWIs used in this test program. Therefore, the carbides in these three samples are more likely to be removed during wear tests.

The point above is also supported by the dependence of wear resistance on the matrix hardness of materials (Figure 7). The wear resistance of these samples displayed a general tendency to increase slowly with increasing the matrix hardness as pct K > pct K_C, indicating the likelihood of a uniform wear-mechanism operating. When pct K < pct K_C, the material loss depends mainly on the removal of unsupported carbides and no such correlation could be found between the wear rate and matrix hardness.

B. *Effects of Dissolved Oxygen Content and Temperature on R_p and E_{corr}*

The effects of DOC and testing temperature on the open circuit potential (E_{corr}) and the polarization resistance (R_p) are summarized in Figure 8. Generally, the polarization resistance of test materials under the aerated condition is much lower than that under the deaerated condition,

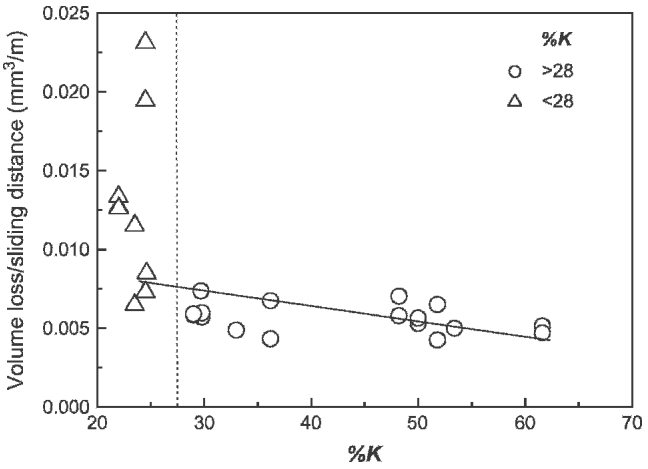

Fig. 6—Dependence of wear resistance on the volume fraction of carbides.

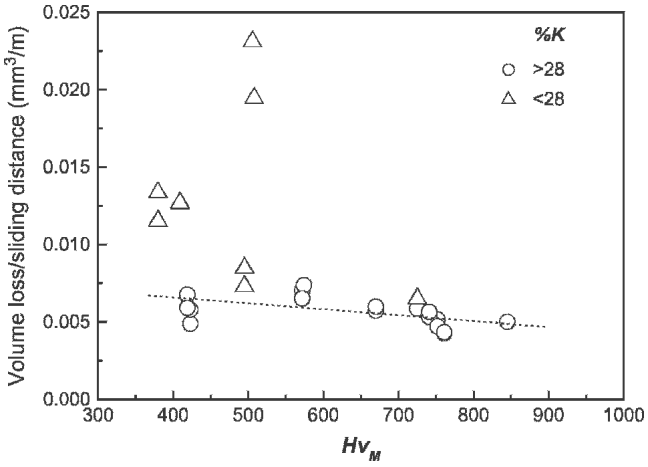

Fig. 7—Effect of hardness of matrix on wear resistance.

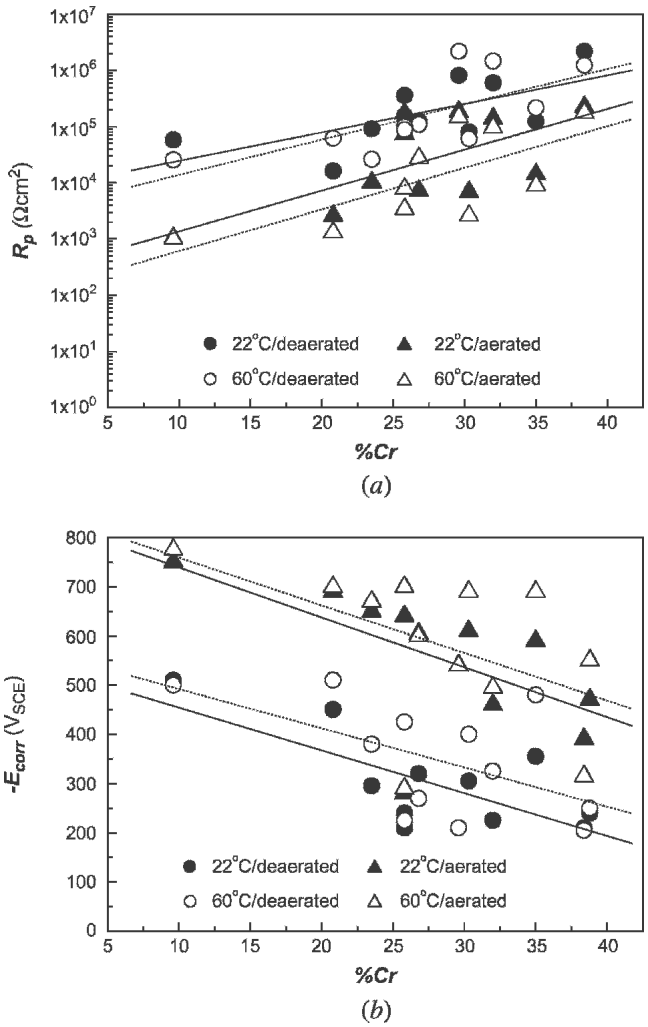

Fig. 8—Effects of DOC and temperature on the (*a*) polarization resistance and (*b*) open circuit potential.

indicating higher corrosion rates under the aerated condition. The corrosion reaction of iron-base alloys in a solution containing dissolved oxygen with near-neutral pH can be written as follows:

$$\text{Anodic reaction:} \quad Fe \rightarrow Fe^{2+} + 2e^- \qquad [2a]$$

$$\text{Cathodic reaction:} \quad O_2 + 2H_2O + 4e^- \rightarrow 4OH^- \qquad [2b]$$

$$\text{Overall reaction:} \quad Fe + 2H_2O + O_2 \rightarrow 2Fe^{2+} + 4OH^- \rightarrow 2Fe(OH)_2\downarrow \qquad [2c]$$

Low DOC due to the deaeration will result in a low rate of cathodic Reaction [2b] and hence a more negative E_{corr}. Since the anodic dissolution rate at the open circuit potential is always equal to the cathodic reaction rate, the dissolution rate of metal will decrease accordingly.

As the temperature is raised from 22 °C to 60 °C, the polarization resistance under the aerated condition decreases with increasing temperature, but it does not change markedly under the deaerated condition. The slight drop of E_{corr} with rising temperature indicates the increasing activity of material.

As indicated by Figure 8, the polarization resistance under the aerated condition increases with temperature. This occurs because the reduced DOC at 60 °C slows the cathodic half-Reaction (2b). Because the anodic and cathodic reactions are always coupled together, the overall corrosion reaction will be decelerated simultaneously. The polarization resistance at the deaerated condition is almost unchanged within the testing temperature range. The reason behind this is that the DOC level under the deaerated condition is very low and the cathodic reaction is likely to be controlled by the hydrogen reduction.

C. *Effects of Chemical Composition on Corrosion Resistance*

It can be seen from Figure 8 that, when the Cr content of CWI is increased, the value of R_p rises and the E_{corr} moves to the noble direction, although the scatter of data is rather large. As shown in Figure 9, both the R_p and E_{corr} decrease when the carbon content is increased.

The corrosion potential of carbide in CWI is believed to be nobler than that of the matrix, and therefore, the corrosion resistance will depend mainly on the corrosion behavior of the matrix.[13,18,19] It is well known that the corrosion resistance of Fe-Cr alloys depends mainly on their free Cr content because the chromium dissolved in the matrix will improve the passivity.[5,19,20] On the other hand, chromium has a stronger affinity to form carbides than iron does, so that a part of the chromium in CWI is consumed in the formation of carbides.[12,21] The amount of carbides will increase with increasing carbon content, and it will reduce the free Cr content dissolved in the matrix, resulting in

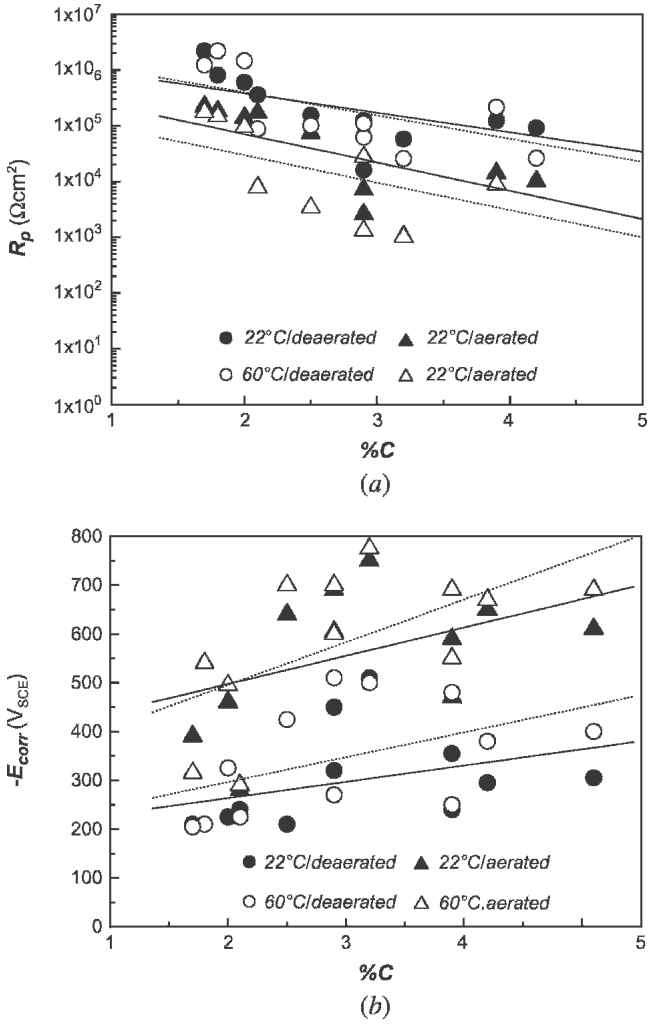

Fig. 9—Effect of carbon content on the (*a*) corrosion resistance and (*b*) open circuit potential.

poorer corrosion resistance. Several types of carbides may coexist in CWI, but most of them, as indicated by Figure 1, are mainly in the form of M_7C_3, where M includes Cr, Fe, and some other carbide-forming elements, depending on the alloy composition.[12,8,17] The percentage of Cr in M_7C_3 increases with the Cr/C ratio of materials.[22,23] Molybdenum, another important carbide-forming element, dissolved in M_7C_3 occupies about one-quarter of the total Mo content in material and Mo_2C consumes another quarter. The rest of the Mo dissolves in the matrix.[17] Summarizing the metallographic analysis results of CWIs with compositions in the range of pct C = 1.95 to 4.31, pct Cr = 10.80 to 25.82, and pct Mo < 3.8, Maratray and Usseglio-Nanot[17] pointed out that the total amount of carbides other than M_7C_3 in these CWI castings is normally less than 1 pct. Consequently, only contribution of M_7C_3 to the chromium distribution in the microstructure is considered to simplify our analysis.

The chromium content of the matrix is approximately estimated with the following procedure. Assume that the CWI is composed of two phases, matrix and M_7C_3, and

denote the chromium content in the matrix and carbide as pct Cr_M and pct Cr_K, respectively. The Cr content ratio α is defined as follows:

$$\alpha = \frac{\text{pct Cr}_K}{\text{pct Cr}_M} \quad [3]$$

The pct Cr_m and pct Cr_k correlate to the weight percent of carbide pct K_W (wt pct) as follows:

$$\text{pct Cr} = \frac{(100 - \text{pct K}_W)\text{pct Cr}_M + \text{pct K}_W \text{ pct Cr}_K}{100} = \text{pct Cr}_M[1 + 0.01(\alpha - 1)\,\text{pct K}_W] \quad [4]$$

where pct Cr is the nominal chromium content of the material. Equation [4] can be rearranged to give an apparent expression for pct Cr_M:

$$\text{pct Cr}_M = \frac{\text{pct Cr}}{1 + 0.01(\alpha - 1)\,\text{pct K}_W} \quad [5]$$

The volume fraction of carbides in the test materials, pct K, can be measured with image analysis, and the results are listed in Table I. The pct K_W can be correlated to the pct K as follows:

$$\text{pct K}_W = \frac{\rho_K}{\rho}\,\text{pct K} \quad [6]$$

where ρ and ρ_K are the densities of CWI and chromium carbide, respectively. Combining Eqs. [6] and [5] and considering $\rho \approx 7.4$ g/cm^3 and $\rho_K \approx 6.7$ g/cm^3,[24] electron probe microanalysis has indicated that the value of α in CWI ranges from 4.3 to 4.8 with an average value 4.55;[22,23] we then have

$$\text{pct Cr}_M = \frac{\text{pct Cr}}{1 + 0.032\ \text{pct K}} \quad [7]$$

Maratray and Usseglio-Nanot[17] proposed an empirical formula to estimate the carbide volume fraction pct K in CWIs:

$$\text{pct K} = 12.33\,\text{pct C} + 0.55\,\text{pct Cr} - 15.2 \quad [8]$$

The data in Figure 10 show that Eq. [8] can give a good estimation for the carbide contents of the test materials with a linear correlation coefficient of $R^2 = 0.977$. The dependence of carbide volume fraction on Cr content is attributed to the solubility of carbon in the iron-based matrix, which decreases with the Cr content.

Substituting Eq. [8] into Eq. [7], the Cr content in the matrix to the nominal Cr and C contents of the material can be correlated as follows:

$$\text{pct Cr}_M = \frac{\text{pct Cr}}{0.51 + 0.39\ \text{pct C} + 0.018\ \text{pct Cr}} \quad [9]$$

The Cr contents of the matrix of the CWIs tested are calculated by Eq. [9] and are listed in Table I. As predicted by Eq. [9], the value of pct Cr_M increases with the nominal Cr content of the material but decreases sharply with the nominal C content (Figure 11) because of the large amount of Cr-containing carbides formed in the microstructure.

The dependences of R_p and E_{corr} on pct Cr_M are shown in Figures12 and 13. The data show clearly that with increasing Cr content in the matrix, the polarization resistance increases and the open circuit potentials move to the noble direction, indicating an improvement of corrosion resistance. In line with the data shown in Figure 12, the relationship between the polarization resistance and chromium content of the materials can be empirically formulated as follows:

$$R_p = R_p^0 \exp\,[\beta(\text{pct Cr}_M)^2] \quad [10]$$

where R_p^0 and β are empirical constants depending on test conditions, and their values are listed in Table III. The

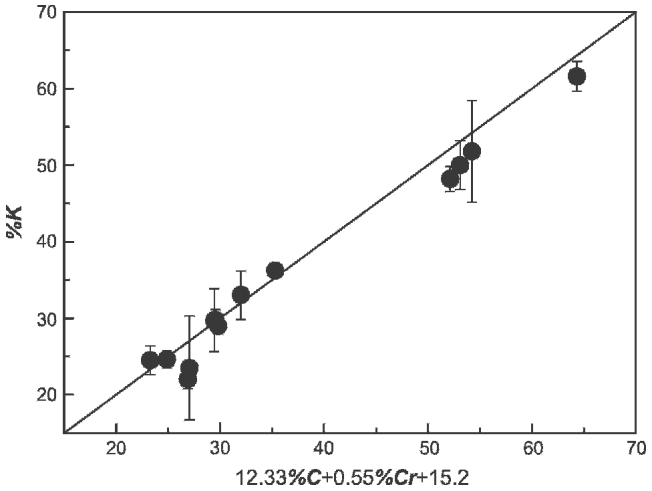

Fig. 10—Comparison of experimental and estimated values of carbide contents.

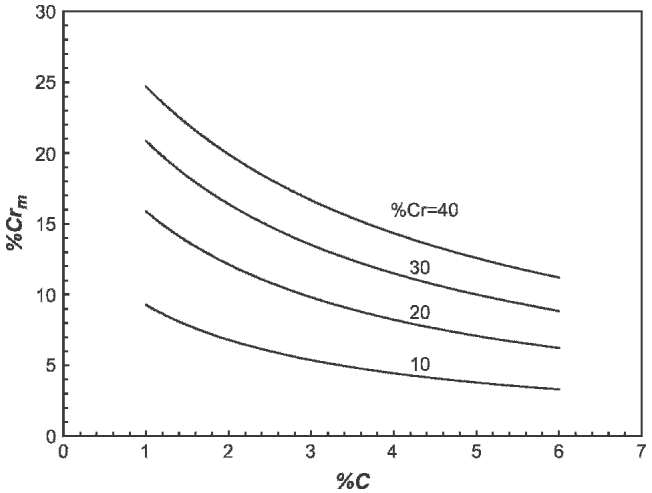

Fig. 11—Dependence of Cr content in the matrix on the nominal Cr and C contents of CWI.

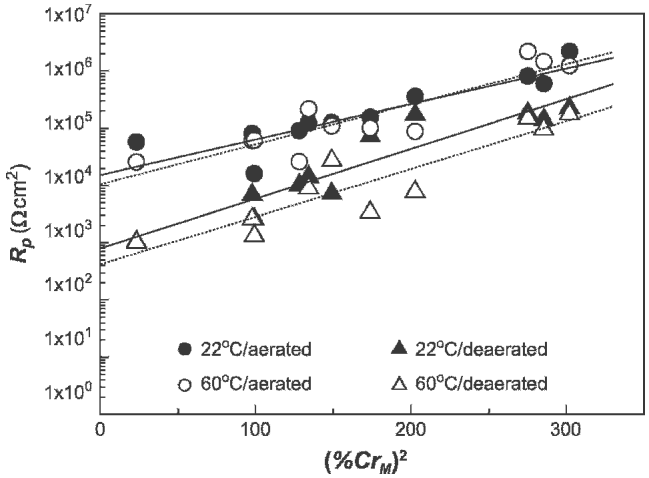

Fig. 12—Effect of Cr content in the matrix on the corrosion resistance.

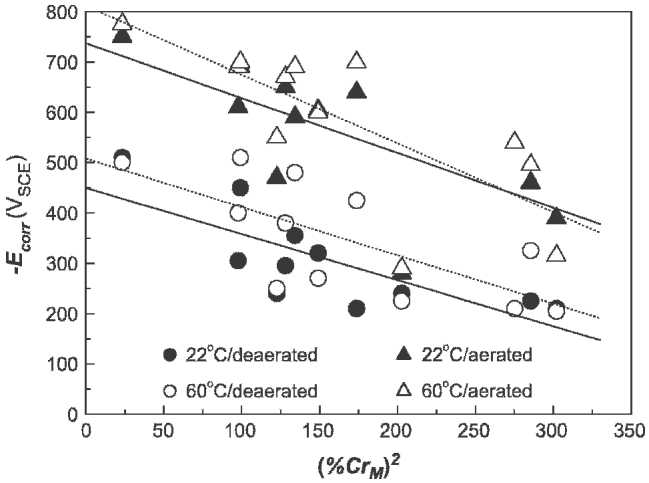

Fig. 13—Effect of Cr content in the matrix on the open circuit potential.

Table III. Values of R_p^0 and β

Test Condition	R_p^0 ($\Omega \cdot cm^2$)	β
Aerated at 22 °C	2,020	0.010
Deaerated at 22 °C	20,400	0.011
Aerated at 60 °C	1,020	0.012
Deaerated at 60 °C	16,200	0.012

coefficient R_p^0 can be regarded as the value of R_p when pct $Cr_M = 0$. The data in Table III indicate that the value of β is essentially independent of test conditions and can be approximately considered as a constant with an average value of 0.011. Consequently, the curves of R_p*vs* pct Cr_M under different test conditions can be approximately normalized with the parameter R_p/R_p^0,

$$R_p/R_p^0 = \exp\ [0.011(\text{pct Cr}_M)^2] \qquad [11]$$

According to Eq. [1], R_p is inversely proportional to the corrosion current density under the open circuit potential,

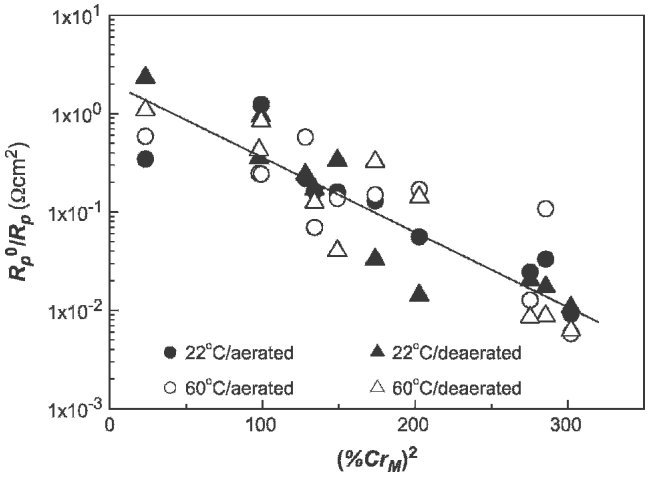

Fig. 14—Normalized curve of the polarization resistance *vs* the Cr content in the matrix.

i_{corr}, so that the normalized curve in Figure 14 is presented in the following form:

$$R_p^0/R_p = \exp\ [-0.011\,(\text{pct Cr}_M)^2] \qquad [12]$$

The parameter R_p^0/R_p is used in the current study to represent the corrosion rate of the material, and its meaning is similar to the weight loss that has been used to represent the wear rate in Section III–A.

Inserting Eq. [9] into Eq. [12], the correlation between normalized corrosion resistance of CWI and its C and Cr contents is obtained as

$$\frac{R_p^0}{R_p} = \exp\left[-0.011\left(\frac{\text{pct Cr}}{0.51 + 0.39\,\text{pct C} + 0.018\,\text{pct Cr}}\right)^2\right] \qquad [13]$$

Generally, the corrosion resistance of CWI is improved by increasing Cr content but is degraded with increasing C content, as shown by Figure 15. Substituting Eq. [7] into Eq. [12], an expression to present the effect of carbide volume fraction (pct K) on the corrosion rate is given as

$$\frac{R_p^0}{R_p} = \exp\left[-0.011\left(\frac{\text{pct Cr}}{1 + 0.032\ \text{pct K}}\right)^2\right] \qquad [14]$$

Figure 16 compares the experimental data with the curves determined by Eq. [14] for pct K dependence of R_p/R_p^0 for CWIs with various pct Cr. Figure 16 indicates that Eq. [14] can give reasonably good prediction for the effect of carbides on the corrosion rate of CWIs. The corrosion resistance of CWI decreases with increasing carbide volume fraction and the effect of carbide content increases with an increase in the nominal Cr content.

D. *Effects of Microstructure on Corrosion Resistance*

In the preceding analysis, only the contribution of carbon and chromium to the corrosion resistance of material was

considered. It is noted that, although Eq. [12] gives a good fit to the data and there is a correlation between the corrosion rate and the Cr content in the matrix, the dispersion of data are rather large. This may be due to the influence of microstructure. To investigate the effect of microstructure on corrosion rate, the data in Figure 12 are replotted according to the microstructure of each CWI, where A is austenite, P is pearlite, and M is martensite. However, the data in Figure 17 shows that it is difficult to identify the influence of matrix structures on the corrosion rate of CWIs. It should be noted that, in the preceding analysis, only the contribution of chromium is considered and the chemical composition is assumed to be uniformly distributed. Actually, the alloying elements other than C and Cr will also affect the corrosion behavior of CWI[13,18] and the segregation often exists in CWIs[22,23] owing to their complex compositions. The segregation can result in significant differences in corrosion resistance.[13,18,19] In addition, Patwardhan *et al.*[13] pointed out that the carbide morphology could also affect the corrosion resistance of CWI. Unfortunately, it is still difficult to evaluate such an effect in a quantitative way.

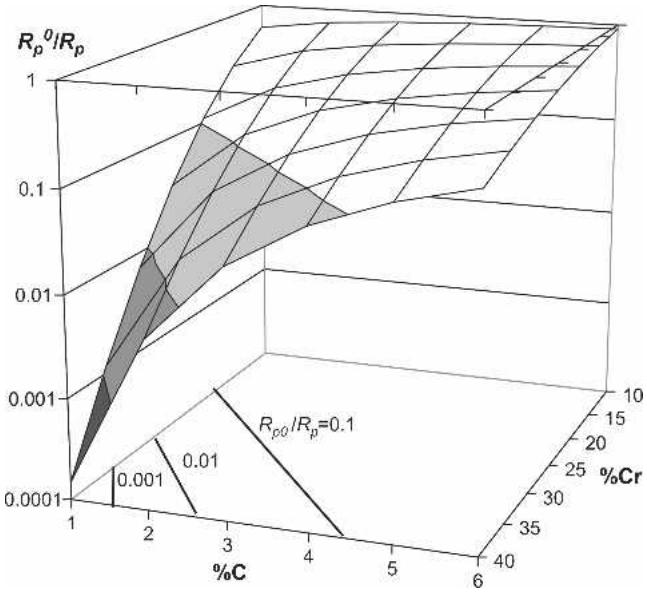

Fig. 15—Dependence of the corrosion rate of CWI on C and Cr contents.

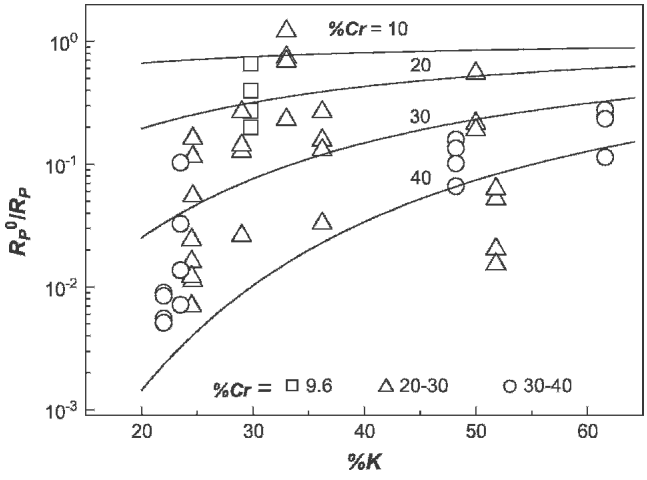

Fig. 16—Effect of the carbide volume fraction on the corrosion resistance of CWIs.

E. *CWIs with a Good Combination of Corrosion and Wear Resistance*

The polarization resistance and average low stress sliding abrasion weight loss of the test materials is correlated in Figure 18. Depending on the performance of the materials, they can be classified as three groups: group I is resistant to wear but not to corrosion, group II displays poor resistance to wear but good corrosion resistance, and group III possesses a good balance of wear and corrosion resistance.

According to the test data depicted in Figure 19, the value of $R_p^0/\mathrm{R_p}$ decreases markedly as pct $\mathrm{Cr}_m > 12$. Such a phenomenon has been well recognized in stainless steels,[20,24] and it indicates that the mechanism for corrosion resistance improvement by adding chromium is similar for both CWI and stainless steel, except that the Cr content

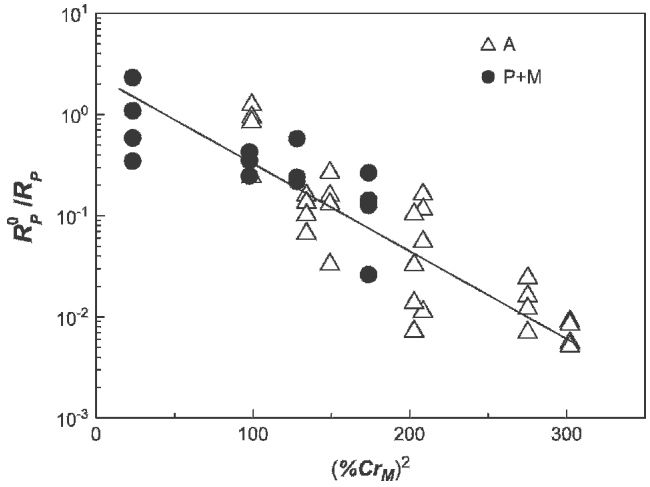

Fig. 17—Effect of matrix structure on the corrosion resistance of CWI.

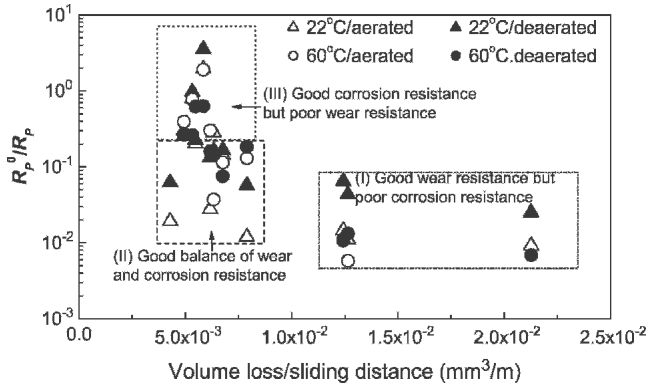

Fig. 18—Interdependence of corrosion and wear resistance.

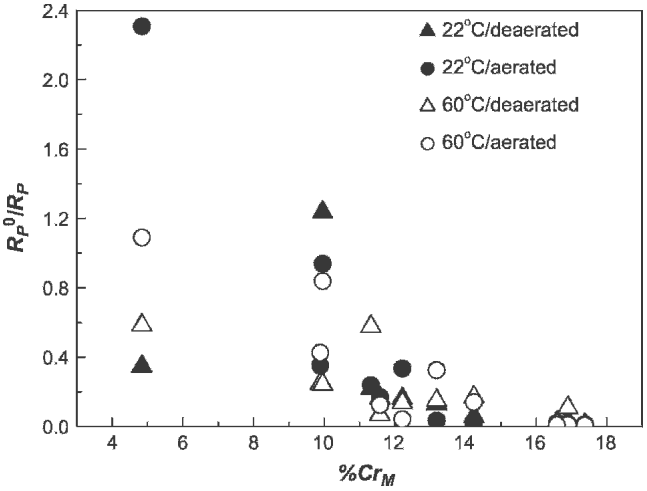

Fig. 19—Dependence of the corrosion resistance on the Cr content in the matrix.

in the matrix should be used to assess the corrosion resistance of CWI. Therefore, if good corrosion resistance is required for CWIs, the Cr content of the matrix should be greater than 12 pct.

According to the test results in Figures 4 and 6, to obtain good wear resistance, the carbon content of CWIs should not be less than 2.2 pct and the carbide volume fraction in microstructure should be greater than 28 pct.

In order to show the relationship between the corrosion resistance and chemical composition of CWI more clearly, the projection of the curved surface of $R_p^0/\mathrm{R_p}$ on the pct C–pct Cr plane is depicted in Figure 20, where the composition points of the test materials are also plotted. It is shown that the composition of materials in group I fall in the region of ($R_p^0/\mathrm{R_p} > 0.2$, pct K > 28), those of group II locate in the region of ($R_p^0/\mathrm{R_p} < 0.2$, pct K < 28, and pct C < 2.2), and those of group III fall in the region of ($0.1 < R_p^0/\mathrm{R_p} < 0.2$, pct K > 28, and pct C > 2.2). The line $R_p^0/\mathrm{R_p} = 0.2$ corresponds roughly to pct $\mathrm{Cr}_m = 12$, as estimated by Eq. [12]. As a consequence, a wear/corrosion performance map shown in Figure 21 is developed to identify alloy compositions that may be suited for wear/corrosion conditions. It can serve as a fast screening tool to identify the wear and corrosion resistance of CWI.

Finally, it should be pointed out that the wear/corrosion performance map is based on the results achieved from the wear test in the noncorrosive environment and the corrosion test in a quiescent solution. Both experimental studies and field observations have indicated that there is a significant synergism of mechanical and electrochemical (or chemical) factors in the erosion-corrosion process, and the contribution of the synergistic effect to the total material loss is so important that it cannot be neglected in practical engineering.[1,25,26] Yue *et al.*[15] have found that when CWI is eroded in a low pH slurry, the contribution of synergism can be as high as 86.3 pct of the total weight loss. Therefore, to evaluate the material performance while erosion and corrosion coexist, the synergist mechanism of erosion and corrosion needs to be better understood.

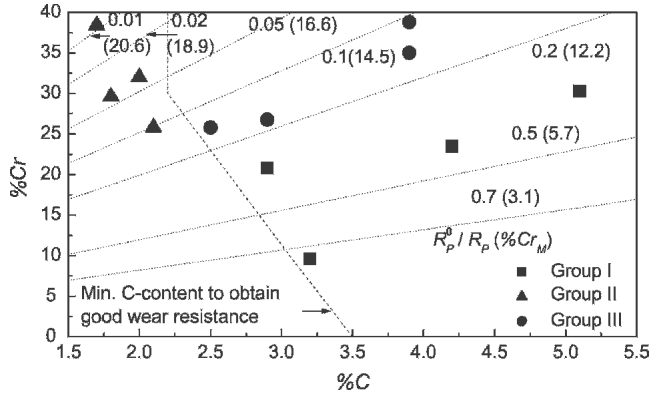

Fig. 20—Dependence of wear and corrosion resistance on C and Cr contents of CWI.

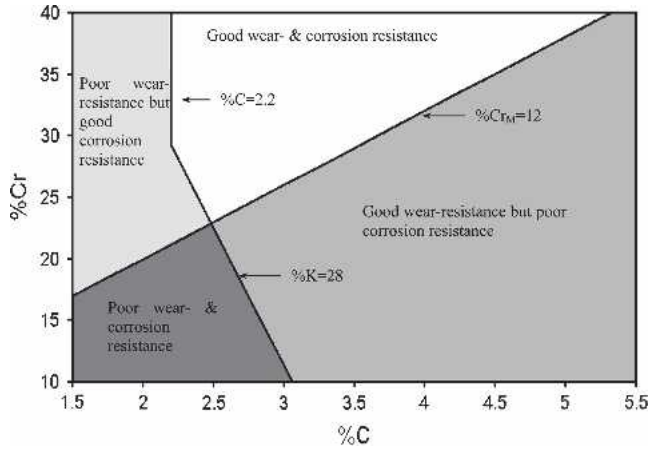

Fig. 21—Wear/corrosion performance map for CWIs.

IV. CONCLUSIONS

1. The resistance of CWI to low stress sliding abrasion against 50/70 Ottawa silica sand increases with the C content pct C or volume fraction of carbides pct K of material. When pct K > 28 and pct C > 2.2, CWI displays a good wear resistance and a weak dependence of wear resistance on the pct K or pct C is observed. When the pct K < 28 or pct C < 2.2, the wear resistance decreases sharply with decreasing volume fraction of carbides.
2. The polarization resistance of CWI in the recycle cooling water solution increases and the open circuit potential moves to the noble direction, with increasing Cr content and decreasing C content.
3. Corrosion resistance of CWI will increase with the drop in DOC, and the effect of temperature on the overall corrosion rate in the aerated tailing solution is controlled by the temperature dependence of DOC.
4. The corrosion resistance of CWI in the tailing solution is mainly controlled by the Cr content in matrix pct Cr_m. When pct $\mathrm{Cr}_m > 12$, the material displays good corrosion resistance.
5. A wear/corrosion performance map is developed to identify alloy compositions that may be suited for wear/corrosion conditions. It can serve as a fast screen tool to identify the wear and corrosion resistance of CWI.

ACKNOWLEDGMENTS

The authors appreciate Dr. H.Y. Ma and Mr. C. Yang for their help in the completing corrosion tests.

REFERENCES

1. H.M. Clark and R.J. Llewellyn: *Wear*, 2001, vols. 250–251, pp. 32-44.
2. C.P. Tabrett, I.R. Sare, and M.R. Ghomashchi: *Int. Mater. Rev.*, 1996, vol. 41, pp. 59-82.
3. T.A. Adler and O.N. Dogan: *Wear*, 1999, vols. 225–229, pp. 174-80.
4. B.F. Levin, J.N. DuPont, and A.R. Marder: *Wear*, 1995, vols. 181–183, pp. 810-20.
5. X. Huang and Y. Wu: *J. Mater. Eng. Performance*, 1998, vol. 7, pp. 463-6.
6. T.A. Adler and O.N. Dogan: *Wear*, 1999, vols. 225–229, pp. 174-80.
7. B.F. Levin, J.N. DuPont, and A.R. Marder: *Wear*, 1995, vols. 181–183, pp. 810-20.
8. R.S. Jackson: *J. Iron Steel Inst.*, 1970, vol. 208, pp. 163-67.
9. H. Oh, S. Lee, J.Y. Jung, and S. Ahn: *Metall. Mater. Trans. A*, 2001, vol. 32A, pp. 515-24.
10. R.J. Llewllyn, S.K. Yick, and K.F. Dolman: *Wear*, 2004, vol. 256, pp. 592-99.
11. O.N. Dogan and J.A. Hawk: *Wear*, 1995, vol. 189, pp. 136-42.
12. C.P. Tabrett, I.R. Sare, and M.R. Ghomashchi: *Int. Mater. Rev.*, 1996, vol. 41, pp. 59-82.
13. A.K. Patwardhan and N.C. Jain: *Metall. Trans. A*, 1991, vol. 22A, pp. 1991-2319.
14. R.B. Davis: *Microstructural Relationship to Flow Accelerated Corrosion, Code and Standard for Quality Engineering*, ASME, Minneapolis, MN, 1994, vol. 285, pp. 3-11.
15. Z. Yue, P. Zhou, and J. Shi: *Wear of Materials*, ASME, New York, 1987, pp. 763-71.
16. L. Valentinelli, T. Valente, F. Casadei, and L. Fedrizzi: *Corr. Eng., Sci. Technol.*, 2004, vol. 39, pp. 301-07.
17. F. Maratray and R. Usseglio-Nanot: *Atlas-Transformation Characteristics of Chromium and Chromium-Molybdenum White Iron*, Climax Molybdenum S.A. Paris, Paris, 1971.
18. V. Kumar and A.K. Patwardhan: *Mater. Performance*, 1993, vol. 32, pp. 66-69.
19. A.F. Zhang, J.D. Xing, Y.M. Gao, and J.Y. Su: *J. Xi'an Jiaotong Univ.*, 2000, vol. 34 (9), pp. 88-91.
20. A.J. Sedriks: *Corrosion*, 1986, vol. 42, pp. 376-89.
21. F. Maratray: *Met. Forum*, 1980, vol. 3, pp. 28-36.
22. G. Laird II: *Trans. Am. Foundrymen's Soc.*, 1994, vol. 102, pp. 497-504.
23. G. Laird II: *Trans. Am. Foundrymen's Soc.*, 1991, vol. 99, pp. 339-57.
24. *Metals Handbook*, Desk ed., J.R. Davis, ed., ASM INTERNATIONAL, Materials Park, OH, 1998.
25. D.D. He, X.X. Liang, S.Z. Li, and H.R. Guan: *Corrosion*, 2005, vol. 61, pp. 30-36.
26. M.M. Stack and N. Pungwiwat: *Wear*, 2004, vol. 256, pp. 565-76.